Journal of Applied Fluid Mechanics, Vol. 18, No. 11, pp. 2810-2822, 2025.
Available online at www.jafmonline.net, ISSN 1735-3572, EISSN 1735-3645.
https://doi.org/10.47176/jafm.18.11.3466

Experimental Study of Water Jet Atomization using the Schlieren Method

B. Fu[1,2 †], Ch. You[1,2], J. Cai[1,2], H. Xiao[1] and B. Lu[2]

[1] *School of Mechanical and Electrical Engineering, Harbin Engineering University, Harbin 150001, PR China*
[2] *Henan Key Laboratory of Underwater Intelligent Equipment, The 713 Research Institute of CSSC, ZhengZhou 450015, PR China*

†*Corresponding Author Email: fubenshaui@hrbeu.edu.cn*

ABSTRACT

The interplay between lateral airflow and liquid jet is extensively utilized in many engineering scenarios, including steam-power gas catapult systems. It is of paramount engineering interest for the fragmentation phenomena of jet in crossflow. This study establishes a jet test system and observes the flow characteristics resulting from water jet and crossflow interaction by utilizing the Schlieren method. The effects of inflow and outflow parameters on water jet penetration depth are extensively examined by evaluating parameters such as the gas-to-liquid momentum ratio, nozzle dimensions, and temperature. This study focuses on jet trajectory patterns and establishes mathematical correlations through penetration depth measurements that yield predictive equations for jet behavior.

Article History

Received February 20, 2025
Revised May 15, 2025
Accepted June 10, 2025
Available online September 3, 2025

Keywords:

Water jet
Gas inflow
Schlieren method
Jet penetration depth
Jet in crossflow

1. INTRODUCTION

The wide engineering application of the crossflow and liquid jet interaction in steam-power gas catapult systems has provided an academic necessity for the study of jet in crossflow and demonstrated its universal practical importance.

The disintegration and vaporization phenomena of jet in crossflow are described as complex multiphase turbulent interactions that involve coupled gas–liquid dynamics, species diffusion, and thermal energy exchange. This scenario encompasses the mutual influence between the injected fluid and surrounding air flow (Gao et al., 2024; Kasmaiee & Tadjfar 2022), particulate breakup mechanisms within the aerodynamic environment, and subsequent phase-change thermodynamics (Li et al., 2021; Yu et al., 2021; Johnson et al., 2024; Zhou et al., 2024). Gao et al. (2024) experimentally investigated the influence of crossflow thermal conditions on liquid jet disintegration dynamics. Their findings revealed that the column fragmentation altitude decreased and the initial trajectory persistence extended as crossflow temperatures became elevated. With the shadow method for measuring parameters including the liquid jet trajectory, Kasmaiee & Tadjfar (2022) investigated the effect of trajectory angles on crossflow dynamics. Their research developed a predictive framework accounting for injection angle variations in liquid jet path modeling. Yu et al. (2021) conducted experimental research on liquid jet disintegration within a supersonic combustion environment. Their methodology incorporated pulsed laser imaging with background illumination alongside a high-velocity spray particle measurement system. This approach enabled detailed observation of transverse jet fragmentation patterns and subsequent droplet size variations for circular and elliptical orifice configurations under crossflow conditions. Zhou et al. (2024) introduced phase Doppler anemometry as an innovative approach for studying atomization phenomena within supersonic combustion chambers. Complementary research by Zhang et al. (2024b) and Zhou et al. (2023) focused on fundamental breakup physics, spray formation mechanisms, and parametric influences on atomization efficiency in crossflow.

Jet penetration depth, surface wave patterns, fragmentation location, droplet size distribution, gas–liquid phase, and velocity distribution are the primary issues on liquid jets in crossflow. Penetration depth serves as a crucial metric for evaluating crossflow jet behavior, and it exhibits dependence on the momentum ratio and dimensionless axial position. Multiple dimensionless parameters, including the Weber number, density contrast, pressure differentials, and Reynolds number, have been incorporated into empirical correlations by various researchers (Chang et al., 2022; Kamin & Khare 2022;

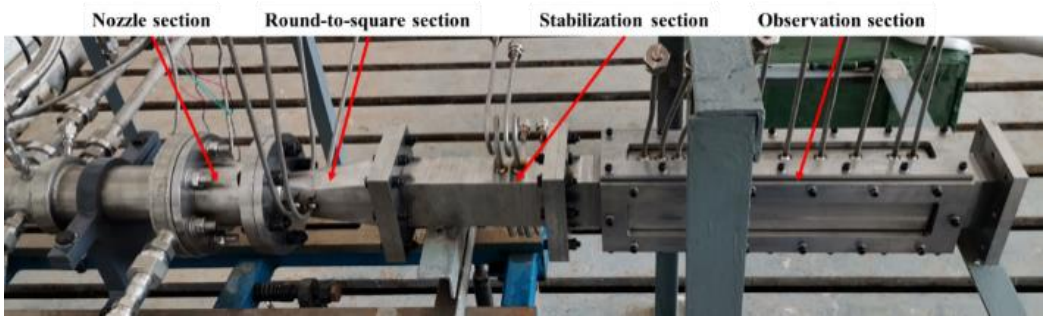

Fig. 1 Jet atomization and evaporation device

Fu et al., 2024; Huang et al., 2024; Xie et al., 2024; Zhang et al., 2024a). Current penetration depth correlations can be divided into three mathematical categories: power law expressions, logarithmic formulations, and exponential relationships. Although considerable research exists on fitting relations, no comprehensive study has been conducted. Chang et al. (2022) investigated the effect of the Weber number and gas-to-liquid momentum ratio (q) on fragmentation processes. This study offered comprehensive analysis regarding the liquid penetration patterns, disintegration positions, and velocity distributions of resulting droplets. Their findings revealed that the q values increased with the reduction in jet curvature and the enhancement in penetration capacity. Xie et al. (2024) developed an integrated theoretical framework that can achieve accurate jet trajectory prediction.

The Schlieren method has been extensively utilized to measure ultrasonic flow fields and other related fields because of its simple operation and high accuracy, with noncontact optical measurement. Focusing Schlieren effectively suppresses disturbances occurring beyond the focal plane while accentuating density variations within the targeted region; thus, it produces exceptional spatial clarity, which makes it particularly valuable for flow visualization studies (Kouchi et al., 2015; Zueva et al., 2020; Yaozhi et al., 2023; Yeganeh et al., 2023; Kathiravan et al., 2024; Lax & Leonov 2024). By integrating two optical approaches, namely, the shadowgraph technique and the Schlieren methodology, Zueva et al. (2020) successfully tracked spray dynamics by monitoring liquid–vapor phase boundaries and fundamental spray dispersion patterns. Yeganeh et al. (2023) developed a synchronized oil injection apparatus combined with Z-configuration Schlieren optics to visualize the dispersion patterns of methane (CH_4) and hydrogen (H_2) fuel. Kathiravan et al. (2024) revealed the influence of jet geometry on combustion performance by using the Schlieren method. Yaozhi et al. (2023) utilized high-frame-rate imaging coupled with Schlieren diagnostics to examine the breakup phenomena of liquid fuel in supersonic crossflows, which helped derive mathematical correlations for spray penetration depth.

This study examines the dynamic relationship between crossflow and water jet within steam-power gas catapult systems. With the aim of determining the influence of external flow conditions on penetration distance and spray patterns, the investigation analyzes fundamental breakup phenomena in high-speed fluid streams. The effect of crossflow dynamics, jet characteristics, and structural variables on the fundamental behavior of water jets is examined, which provides crucial insights for enhancing steam-power gas catapult systems. The study results will have the greatest possible application scope in other fields, particularly in areas such as hypersonic scramjet propulsion systems.

2. EXPERIMENTAL SCHEME

2.1. Experimental System

Considering the fundamental properties of liquid stream atomization, a jet experimental system, which consists of a gas generation unit, a supply apparatus, an experimental bench, a jet atomization and evaporation device, is built. Figure 1 shows the facility elements: nozzle section, circular-to-rectangular transition zone, flow conditioning portion, and visualization area.

The fuel (alcohol) and the oxidizer (oxygen) are delivered from pressurized tanks into the liquid engine. They are ignited in the combustor, and the combustion gas enters the round-to-square section after being accelerated by a Laval nozzle. This geometric modification facilitates the conversion of complex three-dimensional fluid dynamics into more manageable planar flow patterns, which is particularly advantageous for optical diagnostic techniques, including Schlieren. Following the stabilization section, a well-defined two-dimensional velocity profile develops. The accelerated gas stream then proceeds to the visualization area, where liquid is introduced perpendicularly from the lower boundary. Under the influence of the transverse high-velocity flow, the water column undergoes fragmentation and disperses into fine droplets. High-speed Schlieren visualization is implemented within the observation section to capture the detailed breakup characteristics of the aqueous spray.

2.2. Schlieren System

The Schlieren method mainly assists in analyzing flow field properties from the measured deflection angle of light rays. Schlieren techniques can be mainly divided into three types: focusing Schlieren, background Schlieren, and rainbow Schlieren.

Focusing Schlieren revolves around certain positions in different flow fields, which resembles the blurring technique in photography. It produces a clear presentation

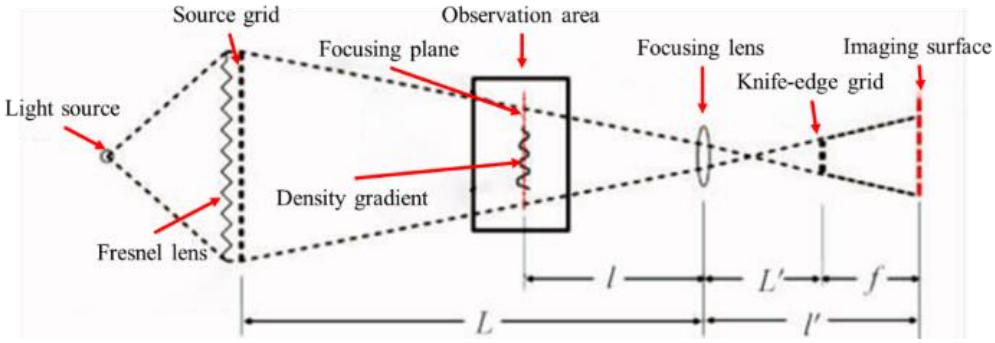

Fig. 2 Optical path of focusing Schlieren

of necessary areas and blurring or fading of unnecessary areas. The focused image obtained can reflect the change in density of the flow field at that position. Integral interferences can be largely eliminated using the focusing Schlieren technique, with only the flow field information of the interested section displayed. Traditional Schlieren imaging is subordinate to a defocused system, in which the Schlieren image mirrors defects, scratches, dust, and other imperfections on the observation window. This condition leads to an inconvenience to the analysis of experimental results. On the contrary, focused Schlieren imaging systems do not encounter such issues.

Focusing Schlieren and conventional Schlieren differ in three main aspects: 1) Conventional Schlieren has a horizontal light path, whereas focusing Schlieren has a conical light path. 2) Conventional Schlieren features only one point light source and one blade; by contrast, focusing Schlieren adopts a source grid and a knife edge grid, which are equivalent to multiple local conventional Schlieren systems. In this context, the source grid is covered with alternating light and dark stripes, and the knife edge grid is generated by replicating the source grid in a certain proportion. The two grids are arranged together. 3) For conventional Schlieren images, the density variation along the entire optical path will "stack" equally on the Schlieren photograph. In focused Schlieren photos, the density changes along diverse sections of the optical path are reflected by different weights. The focused area has a higher weight, whereas the weight plummets outside the focused area. Therefore, density changes are pronounced within the focused area, which is mainly manifested in focused Schlieren photos.

A focusing Schlieren system is divided into three categories—transmission, reflection, and projection—in terms of the overall layout of the system. Compared with the transmission layout, the latter two layout systems overcome the limitation of the Fresnel lens aperture on the observation field to a certain extent. However, the background uniformity of the system is reduced, and background subtraction of the image is usually required.

Figure 2 illustrates the optical path of the transmission focusing Schlieren system. It comprises a light source, a Fresnel lens, a source grating, a focusing lens, a knife edge grating, an imaging system, an image-receiving system, and corresponding supporting brackets. The Fresnel lens converges and irradiates the light emitted by the light source onto the source grid. During nominal functioning conditions, the light-converging optical component resides precisely at the focal region where the radiant energy from the Fresnel element converges. Thus, all the light emitted through the source grid can enter the focusing lens, which maximizes the utilization of the light source. Subsequently, the blade grid is accurately placed at the position of the conjugate image formed by the focusing lens of the source grid. The position of the blade grid is adjusted to ensure that the opaque stripes on the blade grid cut the bright stripes of the conjugate image of the source grid. In the event of a disturbance at a certain point in the test area that causes light deflection, the position of the blade grid will be hindered. Without disturbance, the light can pass through the blade grid to reach the image plane. This system transforms the distribution of density gradients engendered by flow field disturbances (e.g., shock waves, expansion waves, and shear layers) in the test area into the distribution of light intensity and captures it with a camera. In Fig. 2, L indicates the separation between the source grille and the converging lens, L' defines the span from the lens to the knife edge grating, l measures the gap from the examination plane to the optical lens, l' specifies the interval between the lens and the detection surface, and f is the focal length of the focusing lens. The fundamental lens formula $1/f = 1/L + 1/L' = 1/l + 1/l'$ remains valid under these conditions.

This study employs the focusing Schlieren technique to capture large-scale structural features within the dynamic interface between the water jet and transverse air flow. The Schlieren setup consists of several key elements: a laser source, Fresnel lens, source grating, focusing lens, knife edge grating, imaging screen, and high-speed camera. The components are arranged in a certain position, and the observation area is between the source grating and the focusing lens. The relative position relationship is shown in Fig. 3.

2.3. Experimental Conditions

Tables 1 and 2 present several experimental conditions: 10 cold conditions and 10 hot conditions. The abbreviation "gas" refers to the measurements in the entrance and "$water$" to jet parameters. The design variables are given as follows: T* (total temperature), T (static temperature), D_t (throat diameter), D (nozzle diameter), U (flow velocity), We (Weber number), Ma

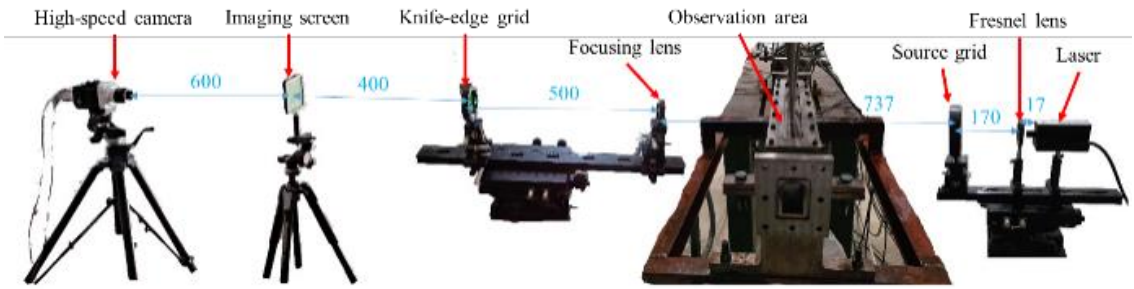

Fig. 3 Relative position relationship of the focusing Schlieren system

Table 1 Experimental parameters under cold conditions

	T^*_{gas}/K	Dt/mm	U_{gas}/m/s	We_{gas}	Ma_{gas}	T_{water}/K	P_{s0}/MPa	P_{s1}/MPa	U_{water}/m/s	D/mm	n	q
C-1	293	14.5	140	74	0.42	293	0.4	0.33	20	3	1	18.3
C-2	293	14.5	140	74	0.42	293	0.5	0.42	25	3	1	25.5
C-3	293	14.5	140	74	0.42	293	0.6	0.50	28.5	3	1	33.3
C-4	293	14.5	140	74	0.42	293	0.4	0.35	23.5	2	1	22.9
C-5	293	14.5	140	74	0.42	293	0.4	0.20	13	5	1	9.0
C-6	293	14.5	140	74	0.42	323	0.4	0.34	22.5	3	1	20.5
C-7	293	14.5	140	74	0.42	293	0.4	0.26	17.5	3	2	12.5
C-8	293	14.5	140	74	0.42	293	0.4	0.15	10	3	3	4.4
C-9	293	17.75	120	64	0.36	293	0.4	0.33	20	3	1	24.1
C-10	293	20.5	110	59	0.33	293	0.4	0.33	20	3	1	29.3

Table 2 Experimental parameters under hot conditions

	T^*_{gas}/K	Dt/mm	U_{gas}/m/s	We_{gas}	Ma_{gas}	P_{s0}/MPa	P_{s1}/MPa	U_{water}/m/s	D/mm	q
H-1	1200	25.1	1000	200	1.85	1.6	1.35	50	3	5.5
H-2	1200	25.1	1000	200	1.85	1.1	0.9	40	3	3.5
H-3	1200	25.1	1000	200	1.85	2.1	1.8	60	3	7.5
H-4	1200	25.1	1000	200	1.85	1.1	1.0	45	2	4.3
H-5	1200	25.1	1000	200	1.85	2.1	1.9	65	2	8.9
H-6	1200	25.1	1000	200	1.85	1.6	1.45	55	2	6.5
H-7	1200	25.1	1000	200	1.85	1.6	0.65	33.5	5	2.8
H-8	1200	20.5	1050	235	1.99	1.6	1.35	50	3	4.2
H-9	1200	17.75	1100	255	2.15	1.6	1.35	50	3	3.8
H-10	2000	25.1	1250	180	1.91	1.6	1.35	50	3	4.4

(Mach number), q (momentum ratio), P_{s0} (water storage tank pressure), P_{s1} (injection pressure), and n (nozzle number).

3. ANALYSIS OF EXPERIMENTAL RESULTS

3.1. Determinants Affecting Jet Penetration Depth

3.1.1. Effect of Water Jet Velocity

Jet trajectories of the experimental conditions C1–C3 when water jet velocity changes are presented in Fig. 4. The Schlieren method is used to obtain the spray paths under the three distinct operational scenarios. The water pressure within the jet tank rises, which leads to alterations in the speed of the fluid stream. Figure 4 shows that, as the velocity of water jet increases, its energy rises under the same experimental parameters. Therefore, it can penetrate more deeply in the same crossflow.

Figures 5 and 6 are the respective images obtained with nozzle diameters of 3 and 2 mm. Under the same experimental parameters, Figs. 5 and 6 demonstrate that the jet speed escalates proportionally with the rise in jet energy levels, which enables effective momentum transfer within identical crossflow conditions. Observations for the setup utilizing a 3 mm nozzle exhibit comparable behavioral characteristics to the setup using a 2 mm nozzle under cold conditions.

3.1.2. Effect of Nozzle Diameter

Figure 7 depicts the jet trajectories obtained using the Schlieren method in the experimental conditions C4 and C5. Under identical water pressure conditions within the storage tank, variations in nozzle diameters result in different outcomes. Figure 7 shows that the jet penetration depth exhibits a proportional relationship with nozzle diameter under the same experimental parameters. The water jet achieves nearly the same energy given the same tank pressure for the water jet storage. The jet attains increased initial speed and reduced deflection angle when a smaller nozzle opening is utilized. Here, the jet decays more rapidly in crossflow, which leads to diminished jet penetration depth. Conversely, a larger nozzle diameter leads to a greater penetration depth.

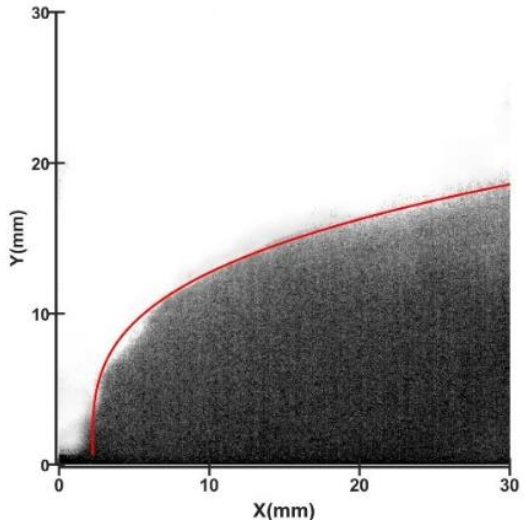

(a) C1

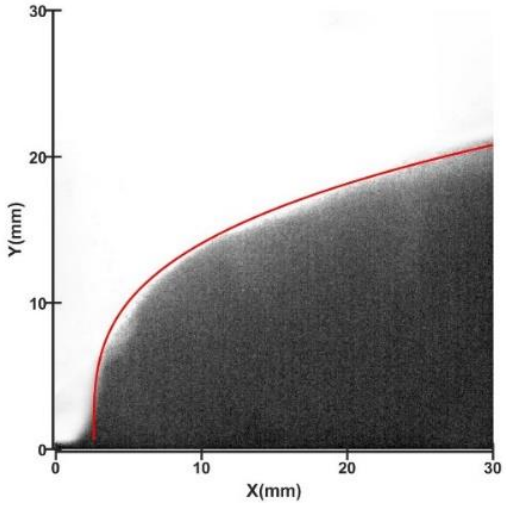

(b) C2

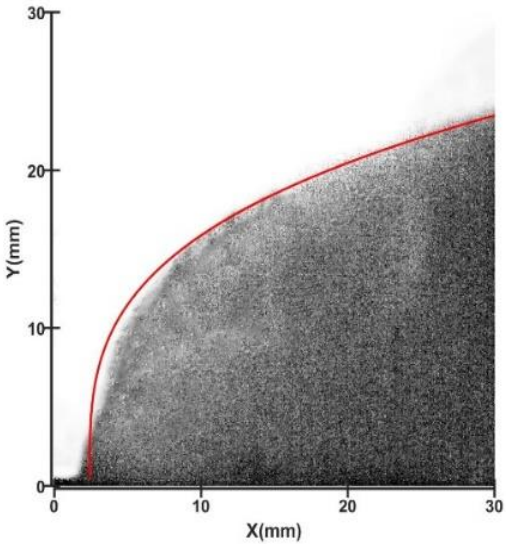

(c) C3

Fig. 4 Trajectory patterns of jet evolution under experimental conditions C1–C3

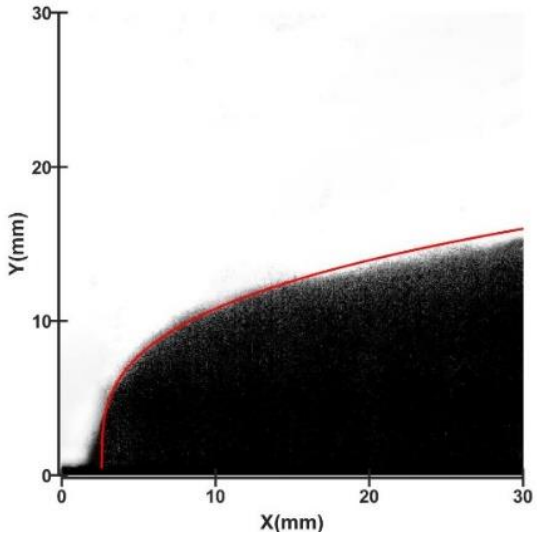

(a) H1

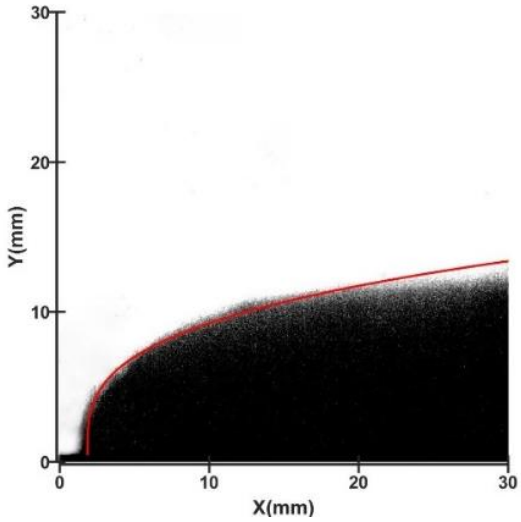

(b) H2

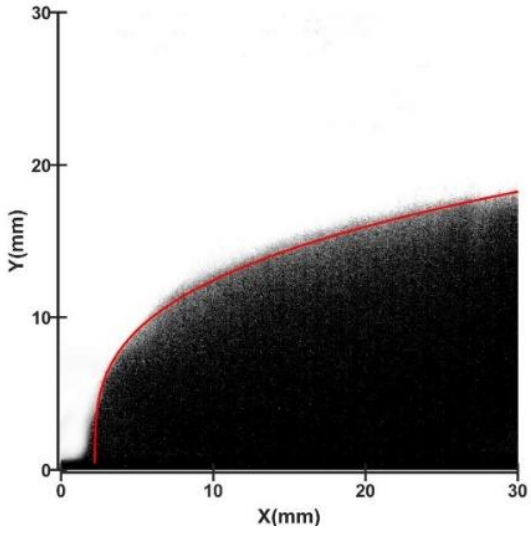

(c) H3

Fig. 5 Trajectory patterns of jet evolution under experimental conditions H1–H3

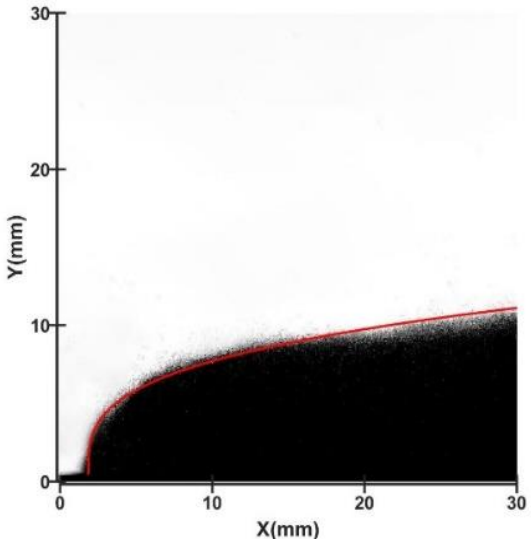

(a) H4

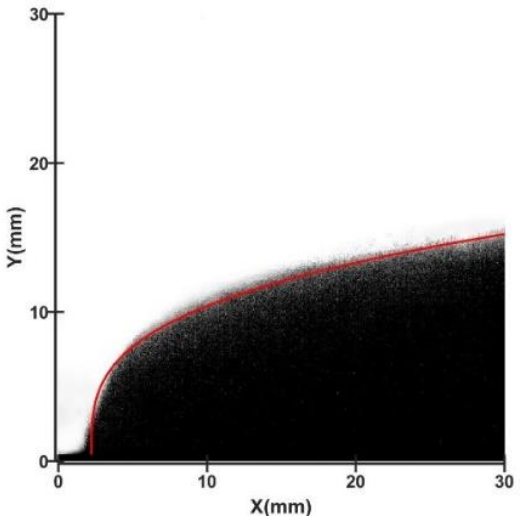

(b) H5

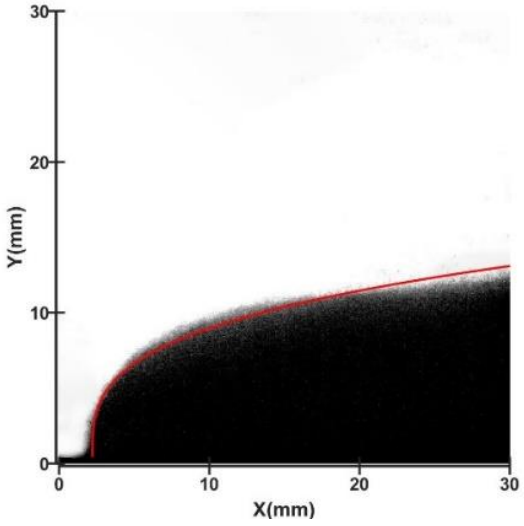

(c) H6

Fig. 6 Trajectory patterns of jet evolution under experimental conditions H4–H6

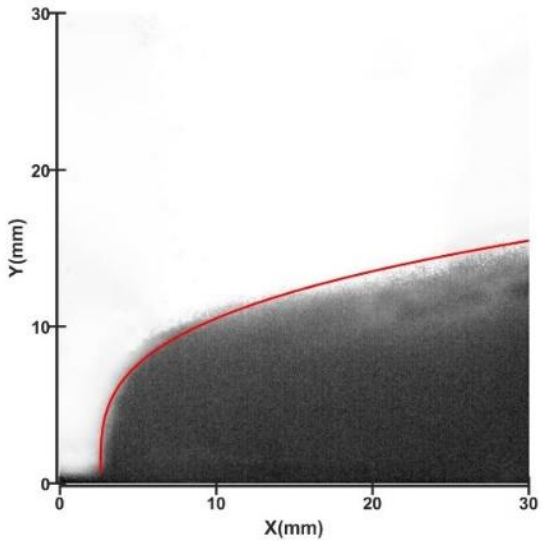

(a) C4

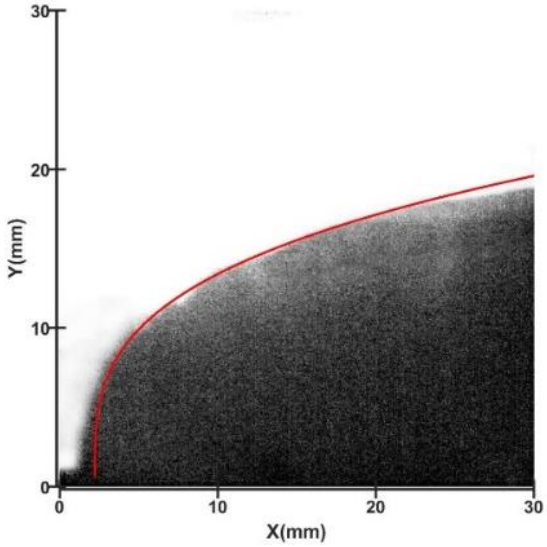

(b) C5

Fig. 7 Trajectory patterns of jet evolution under experimental conditions C4 and C5

As illustrated in Fig. 8, when the pressure inside the water tank does not change, the jet penetration depth increases with the enlargement in the nozzle diameter. This trend coincides with those observed in the cold conditions.

3.1.3. Effect of Water Temperature

Figure 9 demonstrates the path variations of water jets under distinct thermal conditions in cases C1 and C6. The jet penetration depth with the high-temperature water is deeper than that with the low-temperature water.

3.1.4. Effect of the Number of Nozzles

The jet trajectories with varying numbers of nozzles under experimental conditions C7 and C8 are given in Fig. 10. When identical water tank pressure levels are maintained, higher nozzle quantities correlate with reduced injection pressures. Given that water jet speed directly relates to injection pressure, greater nozzle counts

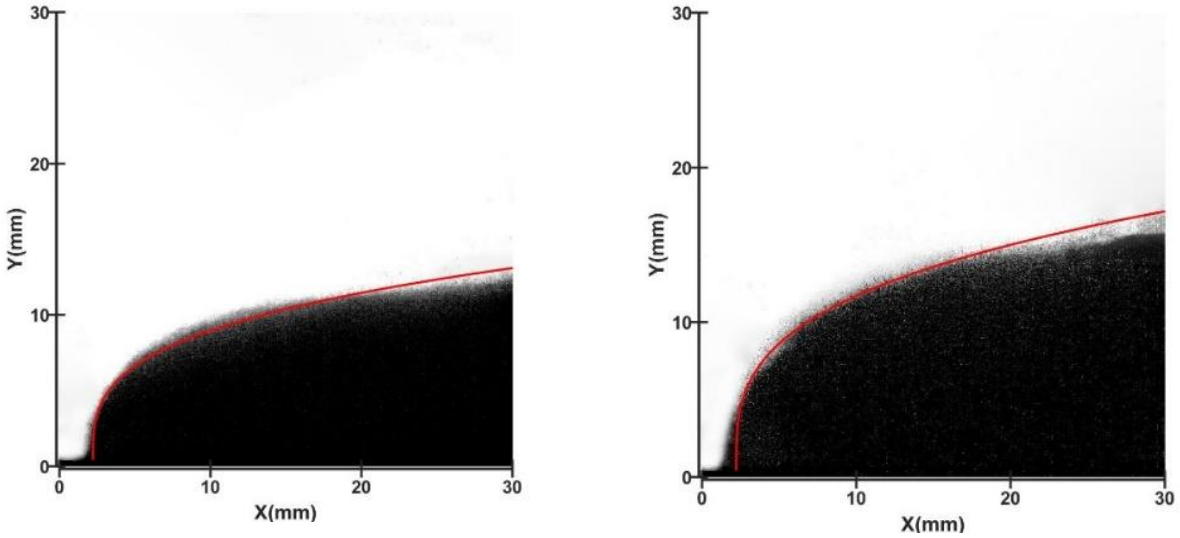

(a) H6 (b) H7

Fig. 8 Trajectory patterns of jet evolution under experimental conditions H6 and H7

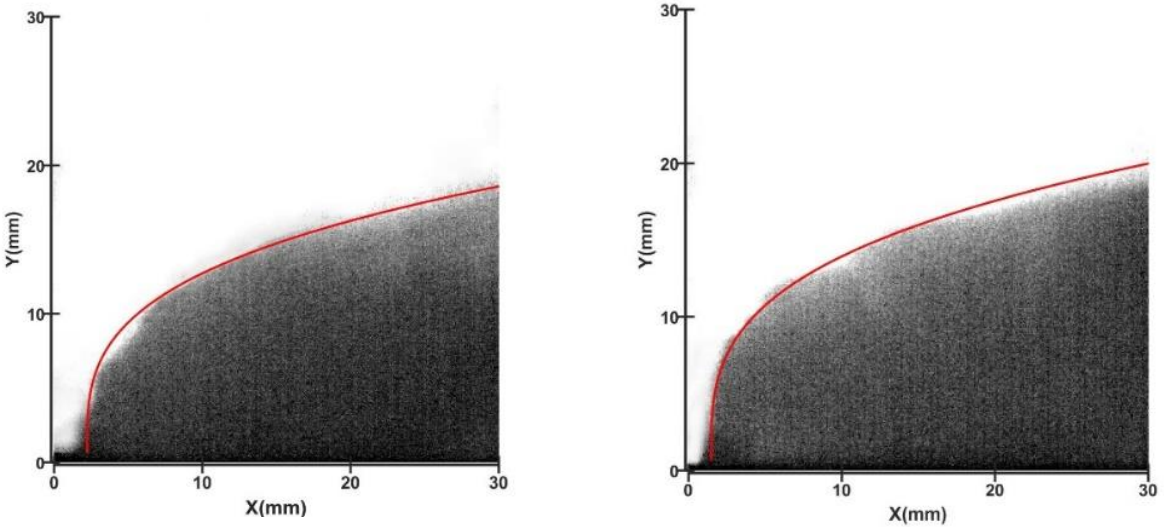

(a) C1 (b) C6

Fig. 9 Trajectory patterns of jet evolution under experimental conditions C1 and C6

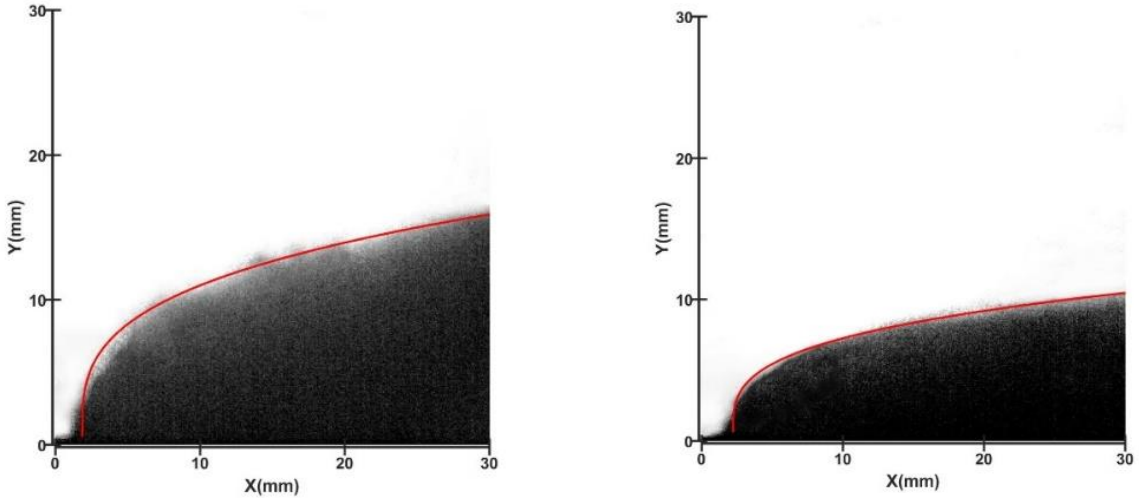

(a) C7 (b) C8

Fig. 10 Trajectory patterns of jet evolution under experimental conditions C7 and C8

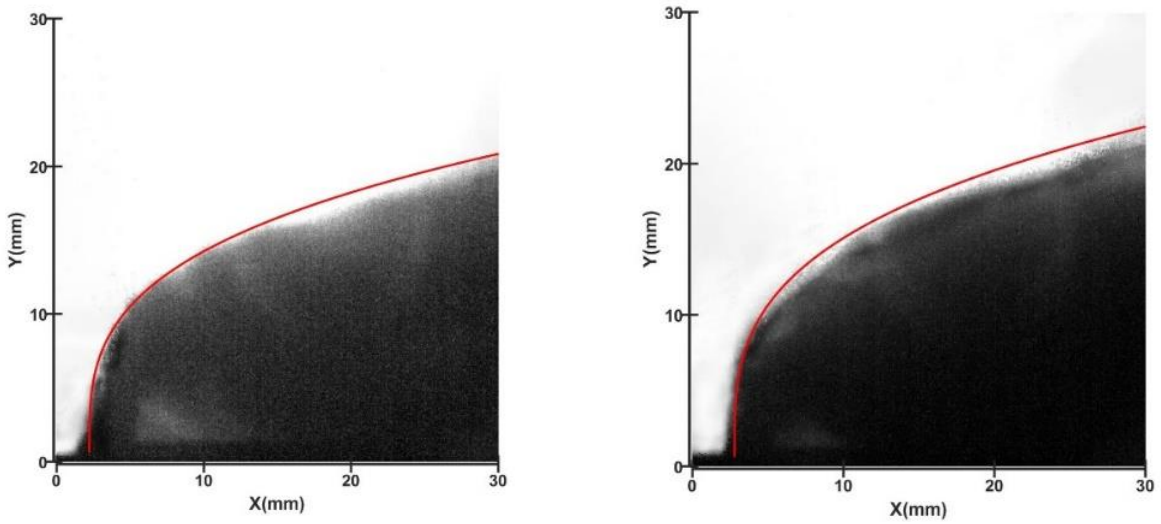

(a) C9 (b) C10

Fig. 11 Trajectory patterns of jet evolution under experimental conditions C9 and C10

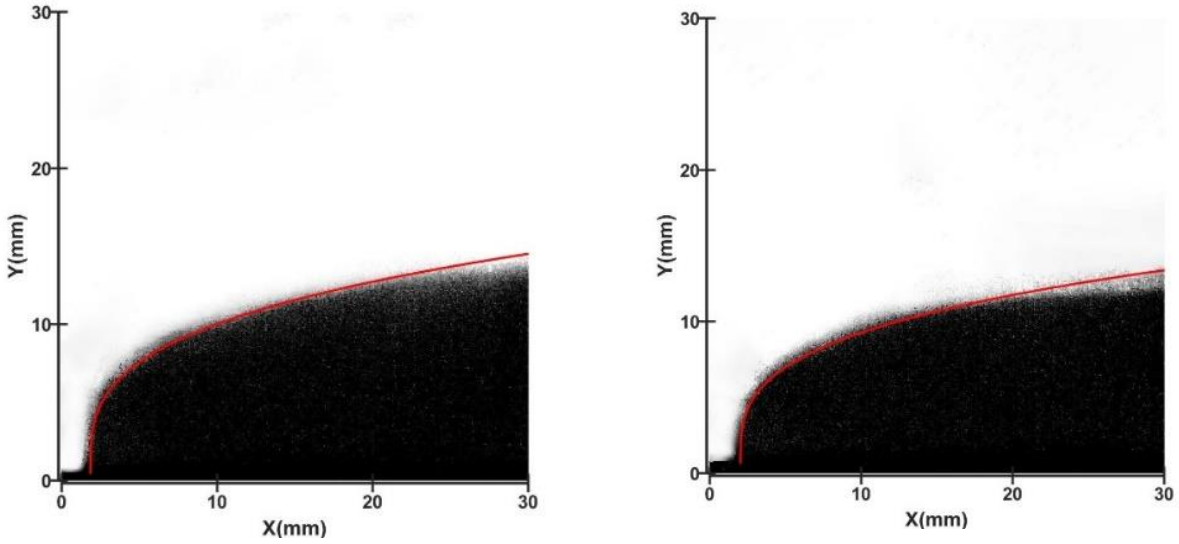

(a) H8 (b) H9

Fig. 12 Trajectory patterns of jet evolution under experimental conditions H8 and H9

consequently, yield diminished jet penetration depths. In scenarios involving multiple nozzles, the crossflow obstruction created by forward-positioned jets causes measurable reductions in the initial deflection angles observed in the rear nozzle.

3.1.5. Effect of Crossflow Velocity

As observed in Fig. 11, the jet trajectories demonstrate a diminished obstruction of the same momentum water jet and an increase in penetration depth with a waning crossflow velocity under the same experimental parameters.

Figure 12 illustrates the trajectory variations of the jet under varying crossflow speeds for conditions H8 and H9. In these conditions, the nozzle dimensions of the liquid propulsion system determine the velocity characteristics. Resistance exhibits a direct correlation with the crossflow speed magnitude. Enhanced resistance corresponds to reduced jet penetration capability. Therefore, an increase in crossflow velocity results in a diminished jet penetration depth.

3.1.6. Effect of Crossflow Temperature

Figure 13 illustrates the jet trajectories observed under experimental conditions H1 and H10 with different oxygen-to-fuel ratios. Considering the limitations of the experimental device itself, the airflow temperature and the velocity are coupled, and the influence of crossflow temperature could not be studied separately. We assume that the primary effect of airflow temperature on the jet is its influence on the evaporation of droplets. We plan to continue conducting in-depth research in this area.

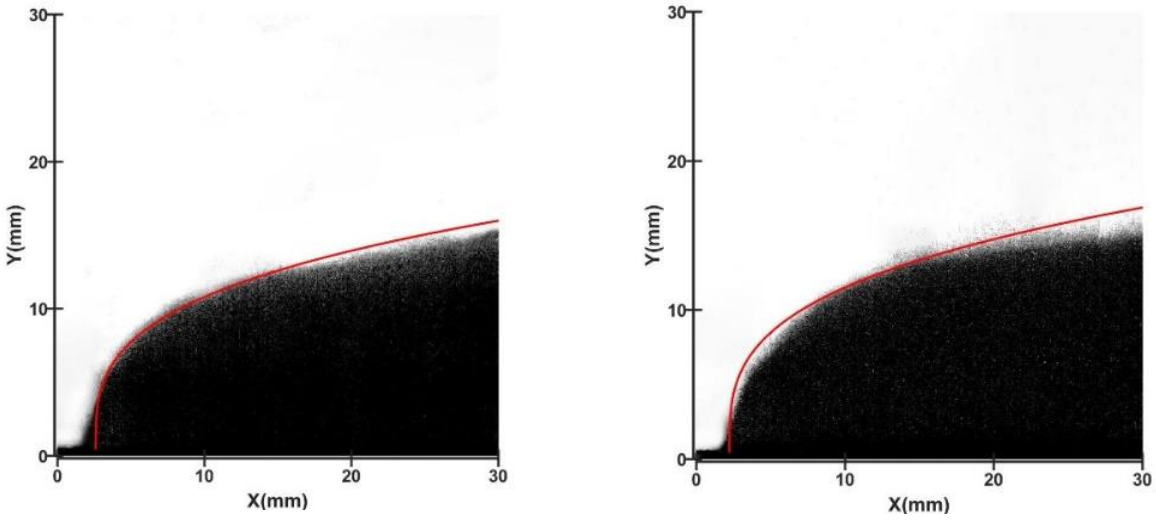

(a) H1 (b) H10

Fig. 13 Trajectory patterns of jet evolution under experimental conditions H1 and H10

3.2. Jet Penetration Depth Fitting

The jet penetration path serves as a critical physical indicator that reflects its developmental progression. It exhibits strong correlations with jet characteristics and crossflow conditions. The general form of jet penetration depth curve prevalent among scholars domestically and internationally is given by (Yaozhi et al., 2023)

$$\frac{y}{d} = Cq^{\alpha}\left(\frac{x}{d}\right)^{\beta} \tag{1}$$

where C, α, and β represent constant parameters.

Equation (1) demonstrates that the jet penetration depth exhibits significant dependence on the momentum ratio between gas and liquid phases. The determination of unknown coefficients involves solving the jet penetration depth equation across varying experimental scenarios. By computing the average of the upper boundary values for the jet path, an approximation of the penetration depth can be obtained. The mathematical formulation describing the jet penetration depth is expressed as follows:

$$\frac{y}{d} = 0.9q^{0.42}\left(\frac{x}{d}\right)^{0.31}\left(\frac{T_g}{T_0}\right)^{0.37}\left(\frac{T_l}{T_0}\right)^{0.2} \tag{2}$$

where d represents the nozzle diameter, q denotes the gas-to-liquid momentum ratio, y indicates the measurement along the trajectory of the water jet, x shows the measurement perpendicular to the crossflow direction, T_g corresponds to the crossflow temperature, T_l reflects the temperature of water, and T_0 serves as the baseline temperature reference.

Figure 14 displays the characteristics of dimensionless jet penetration depth. As evident from the figure, the influence law of jet penetration depth conforms to that described in Section 3.1. The influence law of jet penetration depth without dimensions is remarkably similar to that of jet penetration depth with dimensions, except under working conditions C1, C4, C5 and H1, H6, H7. The influencing factor of the changes in the two groups of experimental conditions is the nozzle diameter. With the change in the diameter, the jet velocity of the jet water changes, which in turn leads to a change in the momentum ratio. Therefore, after applying dimensionless processing with respect to nozzle diameter, the true influence law can be better characterized.

4. CONCLUSIONS

This research employs Schlieren imaging techniques to document jet formation patterns across diverse experimental parameters. The following outcomes are obtained.

1. Using Schlieren, this study establishes an experimental system for jetting, which enables detailed visualization of hydrodynamic interactions between water jet and transverse airflow.
2. Multiple operational parameters including inflow dynamics, thermal conditions, ejection velocities, thermal states, and nozzle dimensions are found to substantially influence jet transformation processes.
3. A predictive model for jet penetration characteristics is derived through dimensional analysis. This model is expressed as Equation (2), which incorporates the momentum ratio and nozzle diameter. These computational results are particularly valuable for optimizing steam-power gas catapult systems.

ACKNOWLEDGMENTS

This work was supported by the Natural Science Foundation of Henan Province (Grant no. 202300410003).

CONFLICT OF INTEREST

No financial or personal affiliations exist that might have biased the outcomes presented in this study, as confirmed by all contributing authors.

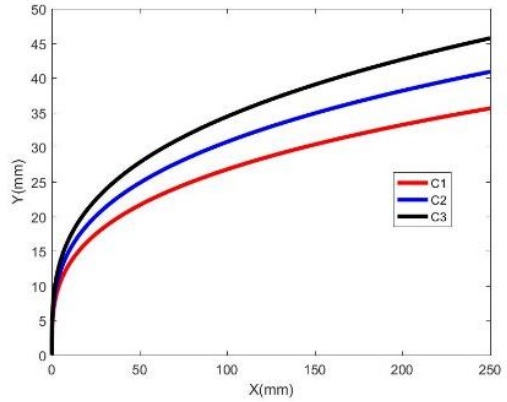

(a) C1, C2, C3

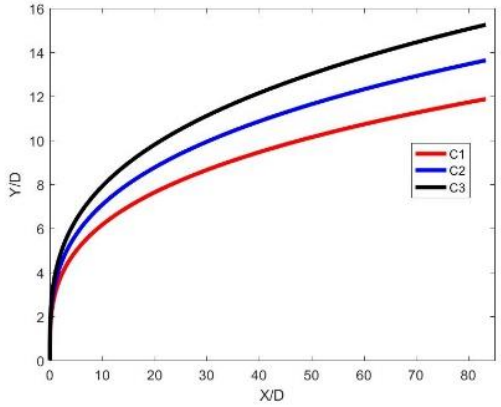

(b) C1, C2, C3

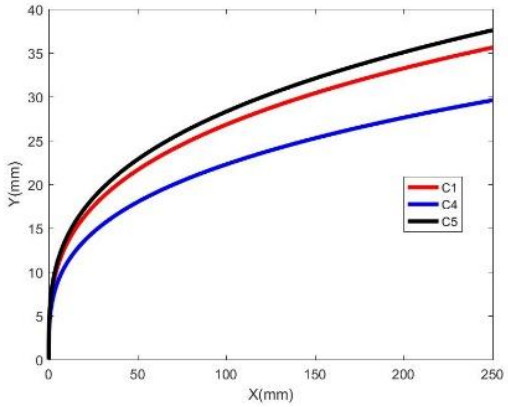

(c) C1, C4, C5

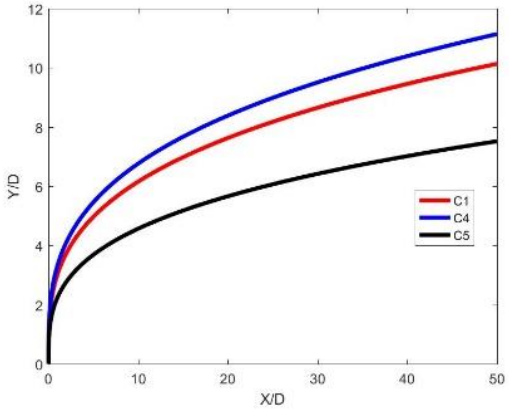

(d) C1, C4, C5

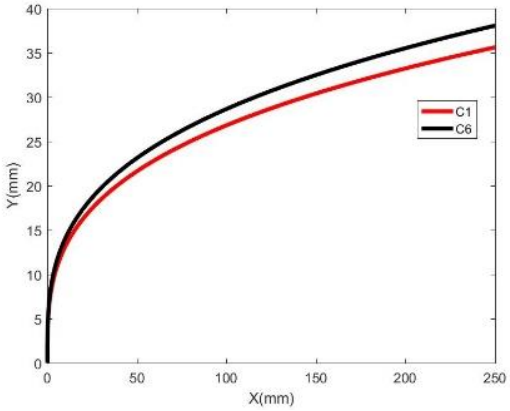

(e) C1, C6

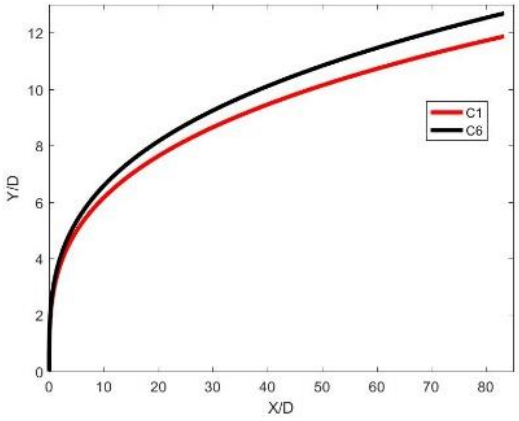

(f) C1, C6

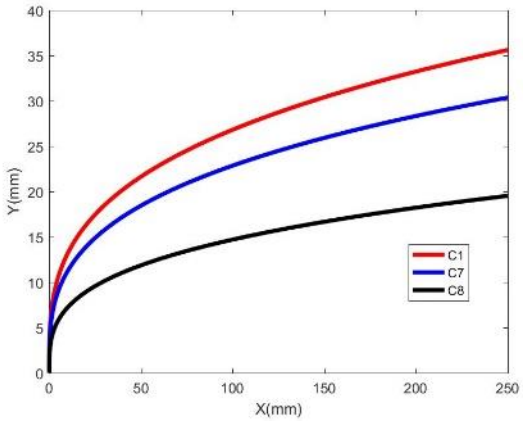

(g) C1, C7, C8

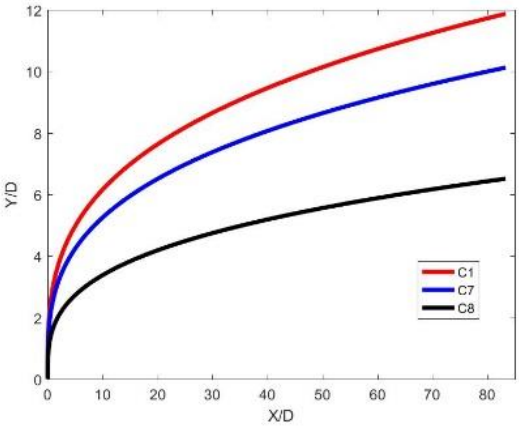

(h) C1, C7, C8

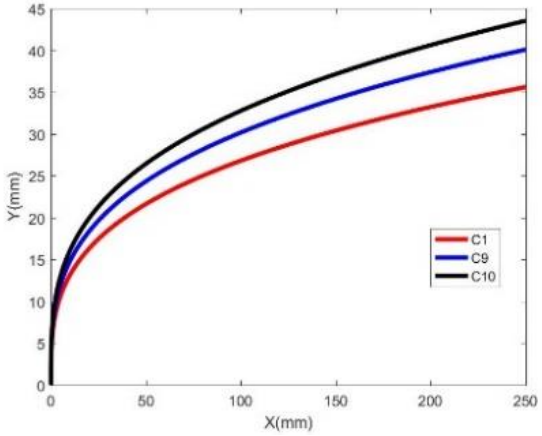

(i) C1, C9, C10

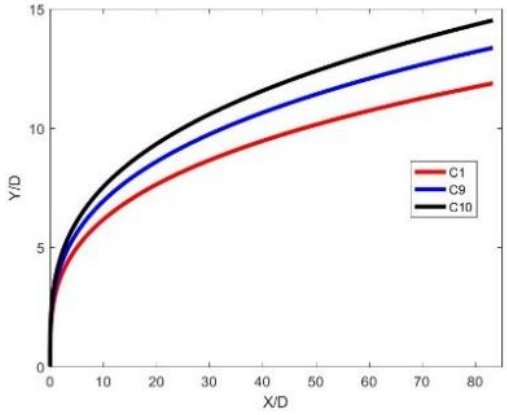

(j) C1, C9, C10

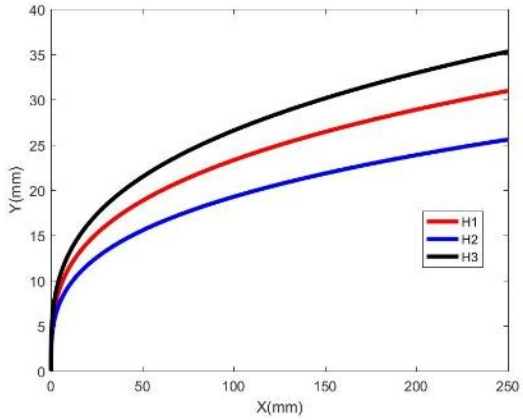

(k) H1, H2, H3

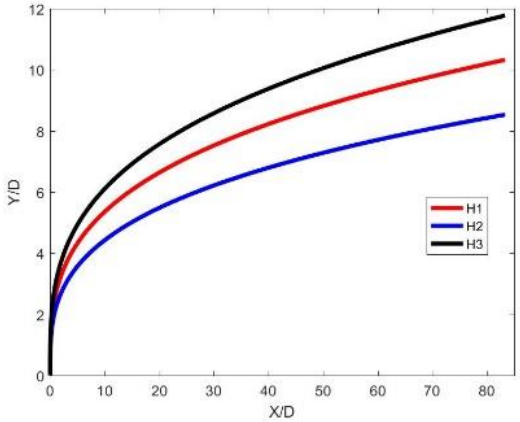

(l) H1, H2, H3

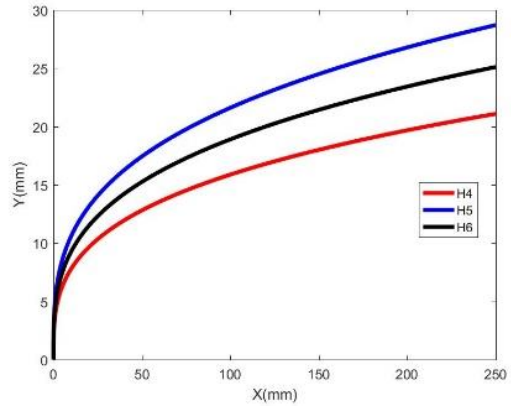

(m) H4, H5, H6

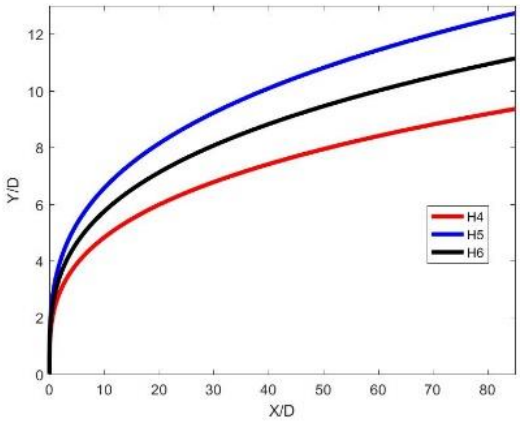

(n) H4, H5, H6

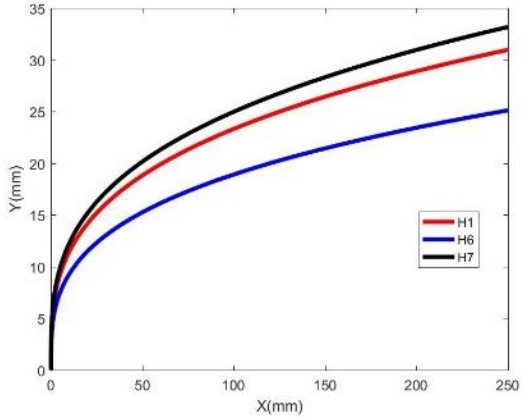

(o) H1, H6, H7

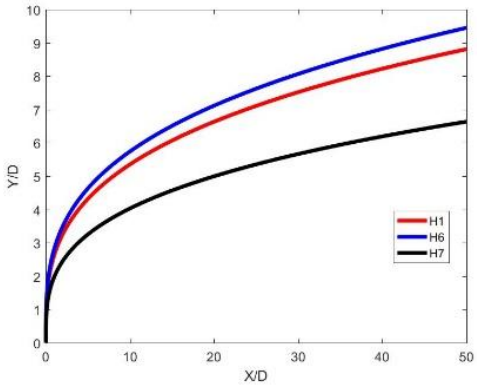

(p) H1, H6, H7

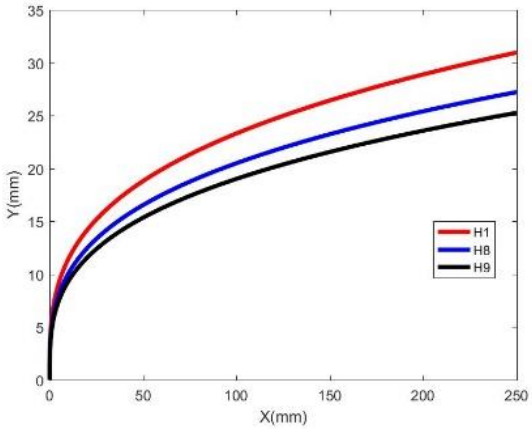

(q) H1, H8, H9

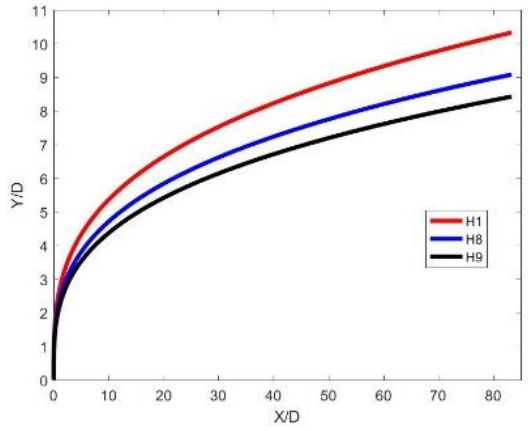

(r) H1, H8, H9

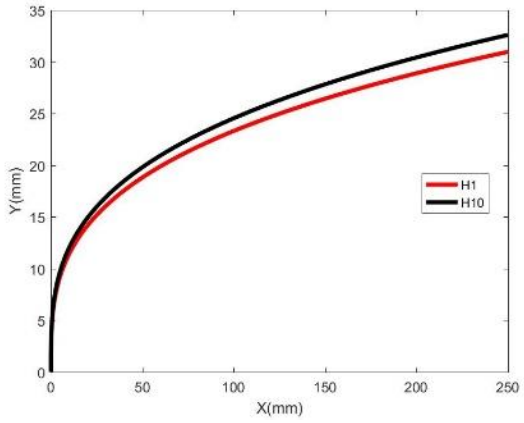

(s) H1, H10

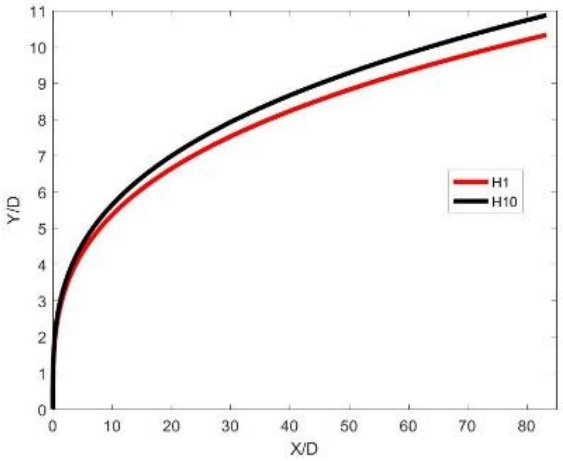

(t) H1, H10

Fig. 14 Comparison of jet penetration depth and dimensionless jet penetration depth curves

AUTHORS CONTRIBUTION

Benshuai Fu: Conceptualisation, Methodology, Data curation, Writing; **Chuang You:** Writing-review and editing; **Jinsi Cai:** Formal analysis; **Haiyan Xiao:** Conceptualisation, Validation; **Bingju Lu:** Methodology, Validation, Supervision.

REFERENCES

Chang, J., He, L., Chen, L., Shen, Z., Chuah, L. F., Bokhari, A., Klemeš, J. J., & Han, N. (2022). Numerical simulation of liquid jet atomization in subsonic crossflow. *Energy*, *257*, 124676. https://doi.org/10.1016/j.energy.2022.124676

Fu, B., Lu, B., Xiao, H., Qin, L., & Li, G. (2024, May). *Experimental research on the atomization of transverse liquid jet*. Journal of Physics: Conference Series (Vol. 2764, No. 1, p. 012049). IOP Publishing. https://doi.org/10.1088/1742-6596/2764/1/012049

Gao, Z., Liu, Y., Liu, G., & Zhang, Q. (2024). Effect of elevated crossflow temperature on jet primary atomization. *Experimental Thermal and Fluid Science*, *111254*. https://doi.org/10.1016/j.expthermflusci.2024.111254

Huang, L., Zhao, K., & Bennett, G. J. (2024). Numerical study of the trajectory, penetration, and interaction of single and tandem jets in a crossflow using LES. *Journal of Aerospace Engineering*, *37*(1), 04023090. https://doi.org/10.1061/jaeeez.aseng-5154

Johnson, J. A., Marsh, A. W., Douglas, E. J., Ochs, B. A., Hammack, S. D., Menon, S., & Mazumdar, Y. C. (2024). Digital holography for the study of non-aerated liquid jets in supersonic crossflow. *Proceedings of the Combustion Institute*, *40*(1-4), 105471. https://doi.org/10.1016/j.proci.2024.105471

Kamin, M., & Khare, P. (2022). The effect of Weber number on spray and vaporization characteristics of liquid jets injected in air crossflow. *Journal of Fluids Engineering*, *144*(6), 061108. https://doi.org/10.1115/1.4053552

Kasmaiee, S., & Tadjfar, M. (2022). Influence of injection angle on liquid jet in crossflow. *International Journal of Multiphase Flow*, *153*, 104128. https://doi.org/10.1016/j.ijmultiphaseflow.2022.104128

Kathiravan, B., Niranjan, S., & Sureshkumar, A. (2024). Experimental investigation on performance of an arc transverse injection in a supersonic combustor flow. *Journal of Applied Fluid Mechanics*, *17*(10), 2169-2180. https://doi.org/10.47176/jafm.17.10.2584

Kouchi, T., Goyne, C. P., Rockwell, R. D., & McDaniel, J. C. (2015). Focusing-schlieren visualization in a dual-mode scramjet. *Experiments in Fluids*, *56*, 1-14. https://doi.org/10.1007/s00348-015-2081-9

Lax, P. A., & Leonov, S. B. (2024). Application of high-speed self-aligned focusing schlieren system for supersonic flow velocimetry. *Aerospace*, *11*(8), 603. https://doi.org/10.3390/aerospace11080603

Li, C., Zhou, Y., Chen, H., & Li, Q. (2021). Cross-sectional droplets distribution of a liquid jet in supersonic crossflow. *Acta Astronautica*, *186*, 109-117. https://doi.org/10.1016/j.actaastro.2021.05.024

Xie, M., Wang, W., Yu, B., He, M., Wu, S., Huang, X., & Liu, H. (2024). Primary breakup model development for trajectory prediction of liquid jets in subsonic crossflow. *Physics of Fluids*, *36*(3). https://doi.org/10.1063/5.0196515

Yaozhi, Z. H. O. U., Zun, C. A. I., Qinglian, L. I., Chenyang, L. I., Mingbo, S. U. N., & Shaotian, G. O. N. G. (2023). Characteristics of penetration and distribution of a liquid jet in a divergent cavity-based combustor. *Chinese Journal of Aeronautics*, *36*(12), 139-150. https://doi.org/10.1016/j.cja.2023.03.006

Yeganeh, M., Cheng, Q., Dharamsi, A., Karimkashi, S., Kuusela-Opas, J., Kaario, O., & Larmi, M. (2023). Visualization and comparison of methane and hydrogen jet dynamics using schlieren imaging. *Fuel*, *331*, 125762. https://doi.org/10.1016/j.fuel.2022.125762

Yu, S., Yin, B., Bi, Q., Jia, H., & Chen, C. (2021). The influence of elliptical and circular orifices on the transverse jet characteristics at supersonic crossflow. *Acta Astronautica*, *185*, 124-131. https://doi.org/10.1016/j.actaastro.2021.04.038

Zhang, C., Lyu, Y., Jiang, L., & Liu, Z. (2024a). Flow Characteristics of Liquid Jet in Transverse Shear crossflow. *Aerospace*, *11*(1), 76. https://doi.org/10.3390/aerospace11010076

Zhang, Y., Tian, Y., & Le, J. (2024b). Review of atomization characteristics of liquid jets in crossflow. *Physics of Fluids*, *36*(2). https://doi.org/10.1063/5.0191630

Zhou, D., Chang, J., Tang, C., & He, L. (2023). Review on research progress in liquid jet in crossflow. *International Communications in Heat and Mass Transfer*, *148*, 107003. https://doi.org/10.1016/j.icheatmasstransfer.2023.107003

Zhou, Y., Li, C., Cai, Z., Li, Q., Li, Z., Chen, Z., & Sun, M. (2024). Experiments investigation on atomization characteristics of a liquid jet in a supersonic combustor. *Physics of Fluids*, *36*(4). https://doi.org/10.1063/5.0204890

Zueva, T. S., Weiss, L., Wensing, M., & Garyaev, A. B. (2020, December). *Experimental investigation of spray propagation under crossflow conditions with Shadowgraph and Schlieren techniques*. Journal of Physics: Conference Series (Vol. 1683, No. 2, p. 022061). IOP Publishing. https://doi.org/10.1088/1742-6596/1683/2/022061